catalysts

MDPI

Article

Upgrading of Bio-Syngas via Steam-CO_2 Reforming Using Rh/Alumina Monolith Catalysts

Woo Jin Lee *, Chaoen Li and Jim Patel

CSIRO Energy, 71 Normanby Rd, Clayton North, VIC 3169, Australia; Chaoen.Li@csiro.au (C.L.); Jim.Patel@csiro.au (J.P.)

* Correspondence: Woojin.Lee@csiro.au; Tel.: +61-3-9545-8375; Fax: +61-3-9545-8380

Abstract: Steam-CO_2 reforming of biomass derived synthesis gas (bio-syngas) was investigated with regard to the steam concentration in the feed using Rh-loaded alumina foam monolith catalysts, which was also accompanied by thermodynamic equilibrium calculation. With 40 vol % steam addition, steam methane reforming and water gas shift reaction were prevailed at the temperature below 640 °C, above which methane dry reforming and reverse-water gas shift reaction were intensified. Substantial change of activation energy based on the methane conversion was observed at 640 °C, where the reaction seemed to be shifted from the kinetic controlled region to the mass transfer controlled region. At the reduced steam of 20 vol %, the increase in the gas velocity led to the increase in the contribution of steam reforming. Comparing to the absence of steam, the addition of steam (40 vol %) resulted in the increase in the production of H_2 and CO_2, which in turn increased the H_2/CO ratio by 95% and decreased the CO/CO_2 ratio by 60%. Rh-loaded alumina monolith was revealed to have a good stability in upgrading of the raw bio-syngas.

Keywords: steam-CO_2 reforming; bio-syngas; rhodium; transition temperature; mass transfer

Citation: Lee, W.J.; Li, C.; Patel, J. Upgrading of Bio-Syngas via Steam-CO_2 Reforming Using Rh/Alumina Monolith Catalysts. *Catalysts* **2021**, *11*, 180. https://doi.org/10.3390/catal11020180

Academic Editor: Leonarda Francesca Liotta

Received: 31 December 2020

Accepted: 22 January 2021

Published: 28 January 2021

1. Introduction

High dependence of energy supply on fossil fuels is leading the world to critical challenges like the issues associated with greenhouse gas emission and the depletion of an energy source [1,2]. According to the recent report from International Energy Agency (IEA) [3], carbon emission has increased by 1.5% in 2018 to a record high of 33.1 billion tonnes, where fossil fuel still accounts for 70% of the rise. This occurs despite renewable energy from solar and wind increases a double-digit growth. Thus, it seems to be obvious that the international regulation and policies for a low carbon footprint will be stringent along with the global target of net zero emission by 2050 [4].

In recent years, as a renewable energy resource the utilization of biomass has gained significant attention, which has been reviewed in terms of overall strategies to produce biofuels [5–7]. Together with other thermochemical routes of biomass conversion such as pyrolysis and liquefaction, the gasification of biomass has been also studied intensively [8] as it produces versatile synthesis gas for the downstream fuel production processes like the Fisher–Tropsch process, methanol and dimethyl ether (DME) synthesis. However, prior to being fed into the downstream, the raw biomass-derived synthesis gas (hereafter, bio-syngas) needs to be conditioned in two aspects: removal of impurities and optimising the H_2/CO ratio as upstream and downstream upgrading processes, respectively.

Removal of typical impurities such as tar and ammonia from the raw bio-syngas has been investigated [9–11] and due to less impact on environments compared to physical separation, hot catalytic gas clean-up process using Ni-based catalysts has been suggested [12]. It is relatively well elucidated how to effectively eliminate those impurities from bio-syngas via physical and thermal pathways [13,14]. For upgrading the bio-syngas to high purity synthesis gas, Chattanathan et al. [15] reported the simultaneous steam and dry reforming of methane using a commercial Ni catalyst in which the maximum methane conversion

with the least coke formation was achieved at 800 °C when both ratios of CH_4/CO_2 and CH_4/steam were 1. Similarly, Wang et al. [16] proposed that the addition of steam in the reforming of bio-syngas enhances the activity and stability of the catalyst dramatically. As an analogous approach to the production of syngas optimized for synthetic fuel, the combined steam and carbon dioxide reforming of methane have been also investigated [17–19]. However, there is still a lack of knowledge on the reaction pathways during the upgrading of bio-syngas that typically contains hydrogen, methane, carbon monoxide, carbon dioxide and steam [20]. Furthermore, considering the recent attention on the utilization of anthropogenic carbon dioxide [21], bio-syngas containing carbon dioxide needs to be properly upgraded using the optimized catalytic system for the downstream fuel manufacturing process for example, which will also contribute to the negative carbon foot print [22].

Monoliths have been extensively investigated as catalyst supporting material in many different applications [23,24]. Recently, monolithic catalysts are gaining more attention as the process miniaturization and intensification becomes the core part in the microreactor technology [25,26]. As mentioned above, raw synthesis gas from biomass gasification usually contains tar and solid particulates, by which the process lines in the downstream are plugged. It was found that monoliths can be operated with gases containing particulates [23]. Monoliths made of refractory materials were found to provide higher activity than normal pelletized catalysts in reforming reactions [24,27]. In view of these advantages, monolith catalysts have been evaluated for the elimination of tar [12,28,29] and gaseous components [16].

The purpose of this study is to investigate the reaction pathways during the reforming of the model bio-syngas that contains typical main components found from the raw biogas. The model bio-syngas in this study does not contain any other particulate impurities and tar. Thus, any effect of these components will not be discussed in this study. In view of their outstanding performance in reforming reactions, aluminium oxide foam monolith and rhodium were chosen as the supporting material and active compound, respectively [30,31]. We have performed the reforming process under the conditions with and without the presence of steam, by which the effect of steam on overall reactions was dealt with in this study.

2. Experimental

2.1. Catalysts and a Model Bio-Syngas

Catalyst used in the present study was Rh/alumina monolith. Rh nitrate (Sigma Aldrich Cat. No. 83750) was dissolved in deionised water to give 0.04 M solution. Alumina foam monoliths (Ceramatec, Inc., Denver, CO, USA, 30 ppi) of 60 mm in length and of 10 mm in diameter were dipped into the solution for 15 min, followed by being dried in an oven at 110 °C for 3 h. These procedures were repeated three times. After being calcined at 550 °C for 4 h in atmospheric condition, it was found that 1.5 wt % Rh_2O_3 (via ICP-OES analysis) has been deposited inside the channel of the monoliths. The methods for the deposition of catalyst on structured material have been well reviewed in the literature [32]. Thus-prepared Rh/alumina monolith was placed in a SiC reactor (Hexoloy SA, Saint-Gobain Ceramics, Latrobe, PA, USA) with two other fresh alumina monoliths stacked up and down. The premixed bio-syngas of $CO/CO_2/CH_4/H_2$/He (28/25/12/33/2 vol %, Coregas Pty. Ltd. Thomastown, VIC, Australia) was used as a model syngas, which referred to the previous study [20]. Helium was used as an internal standard in this study.

2.2. Catalytic Upgrading of Bio-Syngas

Figure 1 shows the schematic diagram of the experimental setup for the catalytic upgrading of bio-syngas in this study. Once the Rh/Al_2O_3 catalyst was stacked with two other fresh alumina monoliths, the reactor was heated to the set temperature in an electric furnace with the rate of 1.67 K min^{-1} under argon flowing. The premixed bio-syngas was fed into the reactor by means of a mass flow controller (Brooks Instrument, model 5890E, Hatfield, PA, USA) without any dilution. Steam addition was operated by a syringe pump

(ISCO Inc., model 260D, Lincoln, NE, USA). Once the temperature was stabilised, argon was replaced by the feed gas and steam. The product gas was analysed using an on-line micro gas chromatograph (Varian, microGC-490, Mulgrave, VIC, Australia), in which a 10 m long PoraPLOT U column and a 10 m long Molsieve 5 Å column were equipped with thermal conductivity detectors. XRD (X-ray diffraction) analyses were performed by using a Bruker AXS D8 advance wide angle X-Ray diffraction instrument with a CuKα radiation source (λ = 1.54056 Å) on the fresh and spent samples together with a blank alumina sample. In the following sections, the net ratio of hydrogen to carbon monoxide represents the net changes in mole fractions as shown in the following equation:

$$\text{Net ratio } H_2/CO = \frac{X_{H2}^{in} - X_{H2}^{out}}{X_{CO}^{in} - X_{CO}^{out}}, \text{ where x is the mole fraction.} \quad (1)$$

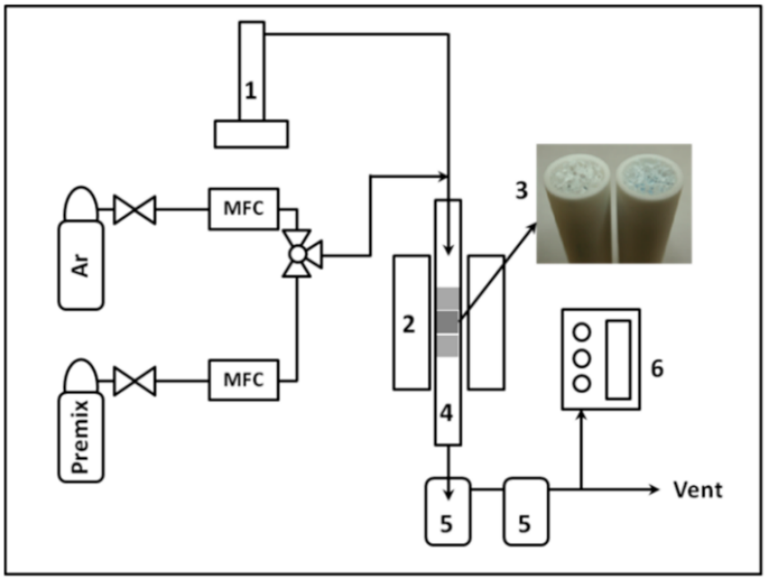

Figure 1. Schematic diagram of the experimental setup for the steam reforming of bio-syngas: (**1**) water pump, (**2**) electric furnace, (**3**) Rh loaded alumina catalyst, (**4**) SiC reactor, (**5**) cold traps and (**6**) a micro-GC.

Non-catalytic operation, which was still with blank monoliths (i.e., without any rhodium addition), has been also evaluated for ensuring that gas-phase contribution was minimised in this study Table 1 shows the materials and reaction parameters investigated in the present study.

Table 1. Materials and reaction parameters.

Alumina foam	60 mm (L) × 10 mm (ø)
Void fraction	0.93
Reactor	α-SiC; 1000 mm in length
Composition of model bio-syngas	$CO/CO_2/CH_4/H_2/He$ = 28/25/12/33/2 vol %
Temperature range	500–1000 °C
Flow rate range	up to 1500 mL min^{-1}
Steam addition	0–40 vol %

2.3. Thermodynamic Analysis

In the present study, the steam CO_2 reforming (SCR) of bio-syngas was simulated by Aspen HYSYS™ software (Aspen Technology Australia Pty Ltd., Melbourne, VIC, Australia). A Gibbs reactor under isothermal conditions was used as the SCR reactor to simulate a set of reactions including R1–R3 at given reaction conditions by solving the heat

and material mass balances, based on minimizing the Gibbs free energy of the components in the reaction set. The Gibbs reactor predicted the product distribution at the chemical equilibrium for the reaction system. The reaction gauge pressure was set at 1 bar. Flow rates of 1000, 1250 and 1667 mL/min were set for the ratio of steam to total feed stream as 0, 20 and 40 vol% respectively. The reaction temperature varied from 500 to 1000 °C with an interval of 50 °C.

$$CH_4 + CO_2 = 2CO + 2H_2,\ \Delta H^0_{298K} = 247.3\ kJ/mol \quad (R1)$$

$$CH_4 + H_2O = CO + 3H_2,\ \Delta H^0_{298K} = 206.0\ kJ/mol \quad (R2)$$

$$CO + H_2O = CO_2 + H_2,\ \Delta H^0_{298K} = -41.0\ kJ/mol \quad (R3)$$

3. Results and Discussion

3.1. Predicted Gas Composition from Thermodynamic Simulation

Figure 2 shows the changes in bio-syngas composition at the equilibrium state in the temperature between 500 and 1000 °C. Feed composition considered for this simulation corresponds to the model synthesis gas as described in the experimental section with the presence of 40 mol% steam. With elevating the temperature, hydrogen composition was seen to steeply increase to reach its maximum at 750 °C and then gradually decreased. Carbon monoxide also increased to 750 °C, where the increase rate became less afterwards. Methane and carbon dioxide decreased with temperature, in which methane was almost completely converted at the temperature higher than 800 °C. Variation in CO_2 fraction was found to be divided into three regions, depending on the slope of the CO_2 removal rate. Below the temperature of 600 °C, CO_2 removal rate was slower than that obtained from the temperature of 600–750 °C where the slope became the highest. Then, the removal rate of CO_2 became minimized at the temperature region higher than 750 °C. The concentration of water decreased rapidly to the temperature of 750 °C, followed by the gradual increase afterwards.

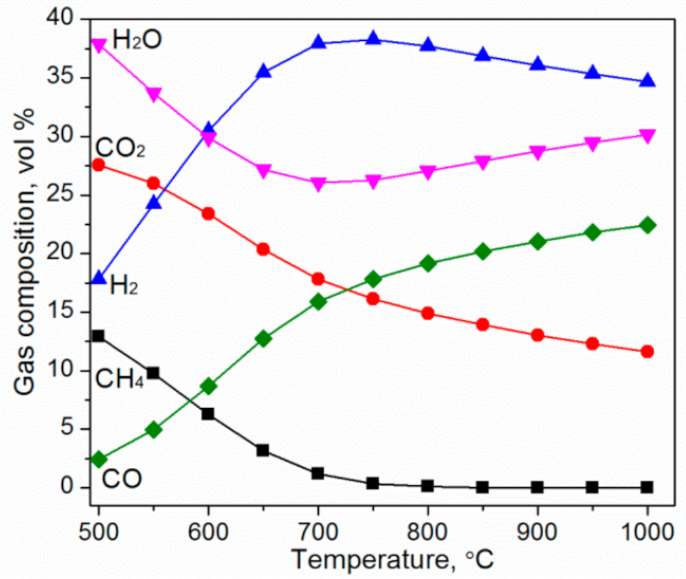

Figure 2. Bio-syngas composition at the equilibrium state in the temperature range between 500 and 1000 °C at 1 bar. Initial feed composition, $CH_4/CO/CO_2/H_2/H_2O$ = 1/2.3/2.1/2.7/5.6 (40 mol% steam).

Combining all these findings, it is expected that the temperature affects significantly the main reactions. Starting from the lower temperature region, where the compositions of H_2 and CO were at the minimum level, the reforming of methane with steam and carbon

dioxide were simultaneously occurred. This leads to the decrease in methane, water and carbon dioxide. However, in the temperature region lower than 600 °C, the consumption rate of H_2O was found to be higher than that of CO_2 due to the water–gas shift (WGS) reaction (R3). The rate of methane reforming diminished as most methane was consumed at the temperature higher than 750 °C. The molar fraction of H_2O reached its minimum at around 750 °C, where H_2 reached the maximum level. After that, it is believed that endothermic reverse WGS (r-WGS) reaction (-R3) was intensified to increase H_2O fraction and decrease H_2 composition.

3.2. Change in the Main Reaction Pathways with Reaction Temperature

Experimental results from catalytic reforming reactions using Rh-loaded alumina monolith catalysts were present in Figure 3. In the temperature between 530 and 850 °C, the methane conversion from catalytic reforming was compared with that from non-catalytic reforming using the alumina monolith without Rh (Figure 3a). While the methane conversion reached more than 80% from the catalytic reforming, negligible CH_4 conversion was achieved from the non-catalytic (i.e., gas phase) reaction. This allowed us to consider that the contribution of non-catalytic reactions during the catalytic reforming reactions was very little. After the reaction, the catalyst surface did contain little carbon on its surface, which was also consistent with the previous study [33]. This further verifies the carbon mass balance in this study.

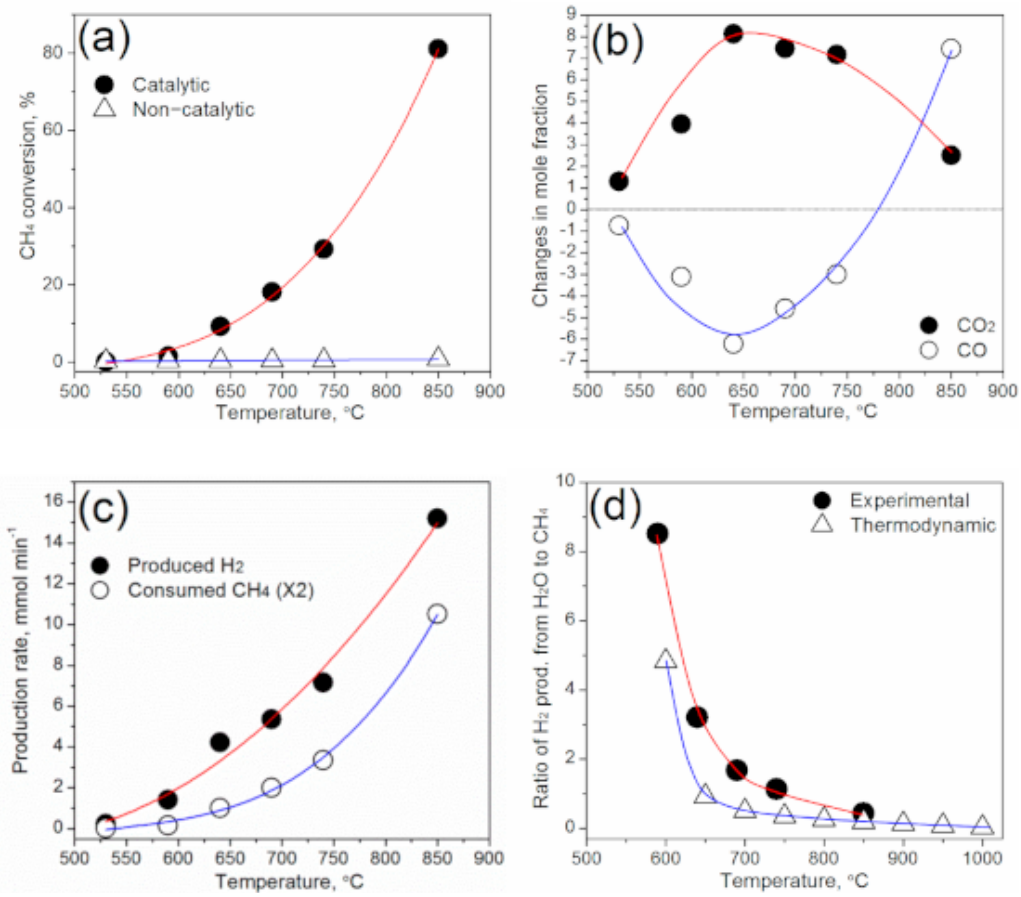

Figure 3. Changes in the steam-CO_2 reforming (SCR) of bio-syngas as a function of temperature at GHSV (Gas hourly space velocity) of 7.6×10^4 h^{-1}, 40 vol % steam and 1 wt % Rh/Al_2O_3 monolith ($Steam/CH_4$ = 5.8). (**a**) Comparison in methane conversion between catalytic and non-catalytic (i.e., blank) run; (**b**) Changes in the molar fraction of CO and CO_2; (**c**) Comparison the produced hydrogen against consumed methane (×2); (**d**) Comparison in contribution of steam and methane to hydrogen production between experimental outcome and thermodynamic calculation in this study.

Figure 3b shows the changes in the molar fraction of CO and CO_2 during the reactions. Positive and negative values at Y-axis represent the production and consumption rates, respectively. It is interesting to note that with increasing the temperature the production and consumption rate of CO and CO_2 changed oppositely. At 640 °C, the consumption rate of CO and production rate of CO_2 were both maximised. As further increasing the temperature, the production rate of CO_2 was gradually decreased whereas the consumption rate of CO was decreased and eventually became positive at 850 °C. At the lower temperature range (i.e., <640 °C), the reactions seem to occur in a way to produce CO_2 and consume CO in overall, where CO_2 conversion through dry reforming is assumed to be very low and WGS reaction is favoured. Consequently, this will increase the overall mole fraction of CO_2 in the effluent. It is also believed that the consumption rates of CO by the WGS reaction (R3) and possibly CO methanation at some extent is higher than the production rate of CO via the reforming reactions (R1 and R2). At the higher temperature range (i.e., >640 °C), as the CO_2 reforming reactions (R1) and endothermic r-WGS reaction (-R3) are both enhanced, the mole fraction of CO_2 started to decrease and simultaneously the consumption rate of CO was decreased. This results in the increase in the mole fraction of H_2O, as also predicted in Figure 2.

To further investigate the reaction routes, the production rates of H_2 were plotted in Figure 3c. Here, the consumption rate of CH_4 was also presented after doubling the original values. Given that all hydrogen atoms produced from methane decomposition are consumed to produce H_2 molecules, the doubled consumption rate of CH_4 will be the maximum production of H_2 from the decomposition of CH_4. From Figure 3c, the overall production rate of H_2 was higher than the maximum production from methane, indicating the contribution from steam. Thus, the production rate of H_2 from steam (r^{H2}_{steam}) can be calculated by subtracting the doubled value of consumed rate CH_4 moles ($r^{H2}_{methane}$) from the overall production rate of H_2 ($r^{H2}_{overall}$). To know the contribution of steam for H_2 production, at least qualitatively, we plotted the ratio of r^{H2}_{steam} /$r^{H2}_{methane}$ against the reaction temperature in Figure 3d. The ratio decreased exponentially with temperature, indicating the decrease in the contribution of steam for overall H_2 production. In addition, the ratio from the experiments was found to be converged on that from thermodynamic calculation. Combining all these results, it is believed that the reactions of methane with steam prevailed over dry reforming under the condition of 40% steam concentration. This is in good agreement with recent studies [34,35], from which the reaction pathways in bio-syngas in relation to steam were investigated. However, it is also obvious that the conversion of methane via dry reforming is intensified with temperature.

The ratio of H_2/CO is a critical factor for the downstream fuel synthesis in that it often determines the overall efficiency of the process [36]. Changes in the H_2/CO molar ratio upon the SCR of bio-syngas is plotted in Figure 4a. The H_2/CO ratio from the experiments increased from 1.2 to 1.9 at the temperature of 640 °C, followed by the gradual decrease to 1.7 at 850 °C, which was close to those calculated from thermodynamic equilibrium. The ratio of H_2/CO approaching to 2, which is desirable to FT synthesis and methanol production, demonstrates that the reforming of bio-syngas under steam addition can produce the tailored syngas ratio for the downstream fuel production. As expected from Figure 3b, the ratio of CO/CO_2 decreased up to 640 °C and then gradually increased towards the thermodynamic values in Figure 4b. The ratio of CO/CO_2 became higher than 1 at 850 °C, which was also known to be beneficial for methanol synthesis using a CO_2-rich syngas [37].

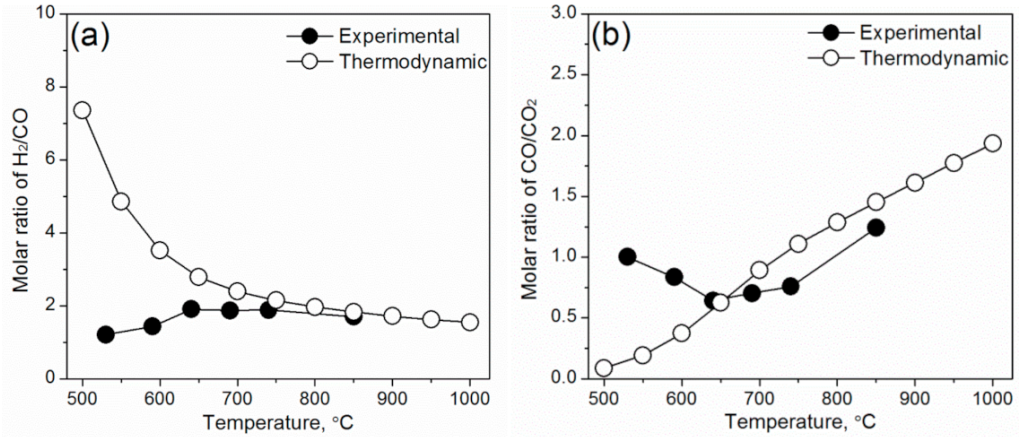

Figure 4. Comparison of (**a**) overall H_2/CO ratio and (**b**) CO/CO_2 ratio between experimental results and thermodynamic equilibrium calculation during the SCR of bio-syngas with 40 vol % steam addition.

3.3. Activation Energy and Transition Temperature

In Figure 5, the turnover frequency (TOF) number based on the conversion of CH_4 over the reciprocal temperature is plotted. It is noteworthy that the slope of the plot sharply changed at 640 °C. In other words, the reaction rate was less affected by the temperature above 640 °C. Such a transition temperature where the slope of Arrhenius plot changes was often observed during the methane conversion reactions in the literature [38–40]. The reported transition temperatures were varied with the conditions employed, being around 350–450 °C when alumina-supported Pd and Pt catalysts were used for the oxidation of methane [38] and 550 °C for Rh/α-Al_2O_3 catalysts used in the partial oxidation of methane [39]. A similar transition was also observed at 500 °C when the Pd/γ-Al_2O_3 wash-coated monolith was used for the combustion of methane [40]. The transition temperature seems to depend largely on the reaction conditions such as the type of catalysts and the feed composition. Appearance of the transition temperature was mainly attributed to the diffusion of the reactant to the catalyst surface. From Figure 5, activation energies revealed from the plot for the low and high temperature region were 299.6 and 87.3 kJ mol^{-1}, respectively. If only internal mass transfer limitation is dominant, the activation energy for the temperature above transition point is half of that for the kinetics controlled region. However, 87.3 kJ mol^{-1} is apparently far less than half of the activation energy (i.e., 150 kJ mol^{-1}) from the temperature below the transition point. It has been suggested that the external mass transfer limitation is attributed to such a sharp drop in activation energy [38,40]. Later experiments combined with the modelling study also suggested that external and heat transfer limitations were responsible for the activation energy lower than half of one from the kinetics regime in exothermic methane combustion [41]. However, in this study the effect of heat transfer limitation would be little as the main reactions are endothermic. Therefore, it is believed in this study that the external mass transfer limitation is mainly responsible for the decline in activation energy above the transition point.

As discussed above, methane reacted mainly with steam in particular for the low temperature range (e.g., $3 < r^{H2}_{steam}/r^{H2}_{methane}$). The activation energy of 299.6 kJ mol^{-1} derived for this temperature range was found to be much higher than those reported from steam reforming of methane in literature as 109 kJ mol^{-1} for 0.4 wt % Rh/Al_2O_3 [42], 169.5 kJ mol^{-1} for 10 wt % Rh/MgO/Al_2O_3 [43] and 240 kJ mol^{-1} for 2–5 wt % Rh/Al_2O_3 [44]. High activation energy from this study is possibly due to the two aspects: methanation of CO/CO_2 and retarding effect due to the copresence of H_2O and CO_2. Panagiotopoulou et al. [45] reported that Al_2O_3-supported Rh and Ru catalysts provided the high activity towards the methanation of CO and CO_2. They have found that when CO and CO_2 were present together, the predominant reaction was methanation of CO at the temperature below 500 °C. Above this temperature, the conversion of CO was found to be decreased

due to the onset of reverse-WGS reaction. Panagiotopoulou and coworkers have also found that the addition of steam did not practically affect the catalytic activity of Rh catalyst but led to the increase in CO conversion due to the WGS reaction (R3). Regarding the retarding effect on the conversion of CH_4, Qin et al. [46] reported that the coexistence of H_2O and CO_2 strongly blocked the active sites for CH_4 activation. These two aspects combined to reduce the conversion of CH_4, which led to the high activation energy in the lower temperature region.

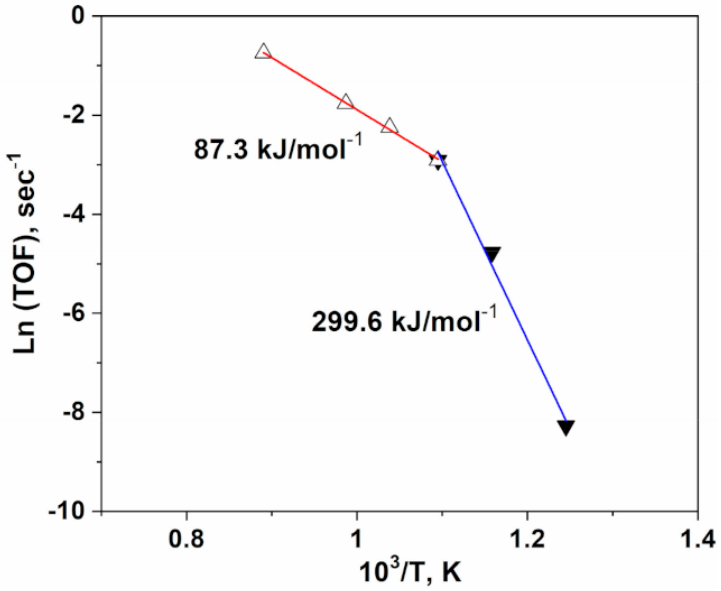

Figure 5. Variation of turnover frequency (TOF) for CH_4 conversion with temperature during the SCR of bio-syngas with 40% steam over the Rh/Al_2O_3 monolith catalyst.

3.4. Effect of Gas Velocity

As described in the previous Section 3.3, the reaction seems to be controlled by the external mass transfer at a high temperature region, which is facilitated by the reduction in the boundary film layer on the catalyst surface. In view of this, the influence of gas velocity on the SCR of bio-syngas was also investigated at 850 °C with 20% steam in this study. Figure 6a shows the consumption rate and conversion of methane as a function of GHSV. Consumption rate of CH_4 was found to be increased as the thickness of film layer was reduced by increasing GHSV. However, due to the fixed length of alumina monoliths in this study, the conversion of methane decreased as a result of the reduction in residence time with the increase in GHSV. As illustrated in Figure 6b, it was found that CO was produced whereas CO_2 was consumed at the condition of 850 °C with 20% steam. The production rate of CO and consumption rate of CO_2 were both enhanced with increasing the GHSV. In comparison to the fact that CO_2 was produced at the same temperature with 40% steam (see Figure 3b), the consumption of CO_2 at 20% steam represents that the dry reforming (R1) was intensified whereas the WGS reaction (R3) was reduced. Simultaneously, the r-WGS reaction (-R3) will be thermodynamically favoured at this high temperature. This also led to the decrease in the production of H_2, as shown in Figure 6c, where the production rate of H_2 was very closer to the doubled amount of consumed CH_4 compared to Figure 3c. Consequently, the overall H_2/CO ratio was reduced (1.7→1.2) in comparison with that from the condition of 40% steam with GHSV of 7.6×10^4 h^{-1} as shown in Figure 4a.

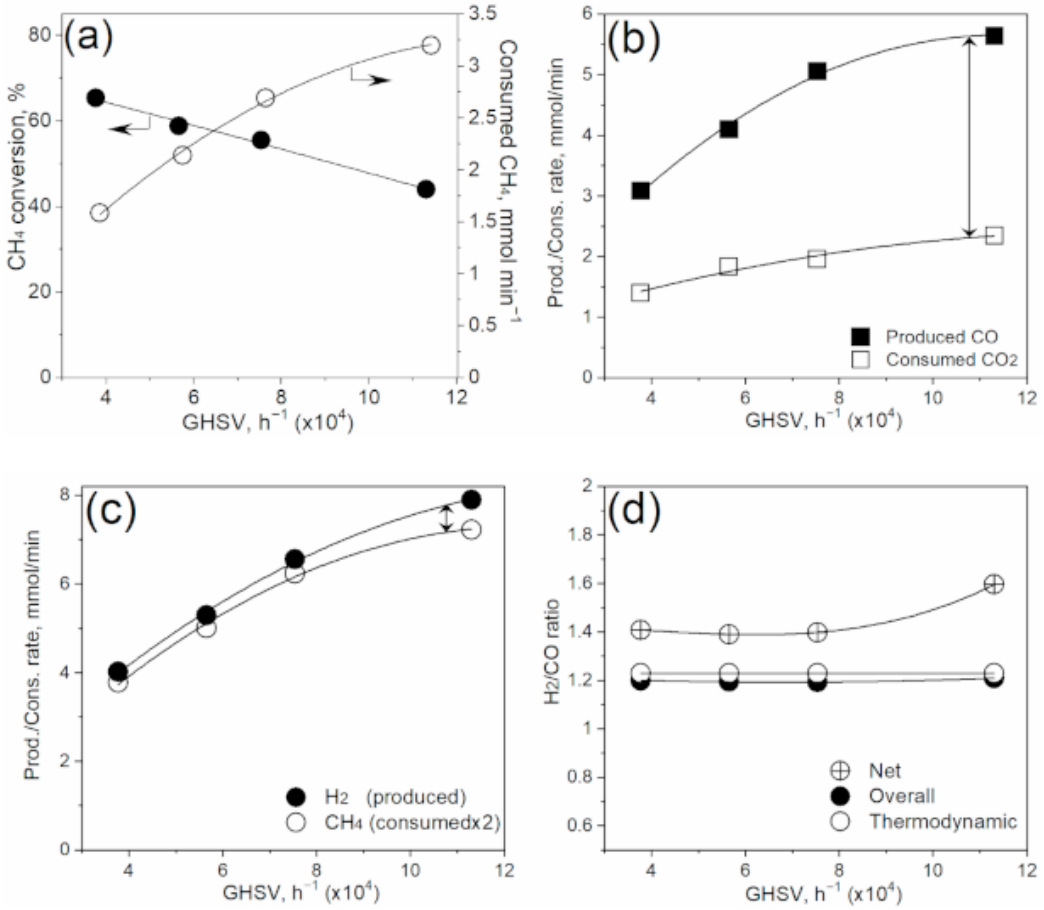

Figure 6. Changes in the reforming reaction of bio-syngas with 20% steam as a function of the gas space velocity at 850 °C. (**a**) Methane conversion and consumed rate of methane; (**b**) Production/consumption rate for CO and CO_2; (**c**) Production/consumption rate for H2 and CH_4 (×2); (**d**) Changes in H_2/CO ratio.

It is also noticed in Figure 6b,c that when GHSV increased, more CO and H_2 were produced in consideration of the consumed amount of CO_2 and CH_4 (indicated by arrows). This implies that more steam is involved in the reforming reactions to produce CO and H_2 with increasing GHSV. It seems that the contribution of steam in the reforming of methane was intensified and simultaneously that of the r-WGS reaction was decreased. According to the previous studies [30,47], it is generally agreed that the consumption rate of CH_4 through steam reforming is faster than that through dry reforming. It was also reported that the CO_2 conversion was considerably retarded when steam was added as a co-oxidant [48]. This phenomenon seems to be intensified with increasing the gas velocity, based on the result in this study. In other words, steam reforming is less affected than dry reforming by increasing the gas velocity. It is believed that more CH_4 tends to convert by means of oxidising species (i.e., O* or OH*) generated from H_2O than that from CO_2 with the reduction in the residence time.

It was found that the overall H_2/CO ratio has not been affected by changing the gas velocity in this study. As shown in Figure 6d, overall H_2/CO ratio remained constant at around 1.2, which is close to that from the equilibrium value. However, with increasing GHSV, the net H_2/CO ratio increased with being diverged from the equilibrium value, which is in good agreement with the previous report [49].

3.5. Effect of Concentration of Steam in the Feed

Table 2 shows the effect of steam concentration on the SCR reaction of bio-syngas. Methane conversion was enhanced with the addition of steam in the feed. Considering

the changes in mole fraction for each component, the main pathway to convert methane seemed to substantially change. With the absence of steam, CO_2 consumption was almost twice higher than that of methane, indicating methane conversion mainly occurs via dry reforming. In addition, CO production was maximised due to the prevailed R-WGS. As a result, the change in H_2 mole fraction was only 6.6, which was half of the expected value (12.3) from CH_4 decomposition. With 20% steam addition, where methane steam reforming was intensified and the R-WGS was suppressed, the production of H_2 increased (6.6→13.8) while the consumption of CO_2 decreased (−11.9→−4.8). At the highest steam concentration of 40% in this study, the net change of CO_2 eventually became positive, i.e., the production. With the change of steam concentration, the ratios of H_2/CO and CO/CO_2 have substantially changed. It was seen in Table 2 that H_2/CO ratio has increased from 0.39 to 3.78 on the basis of their net changes in mole fractions. For the overall ratio, it has increased from the feed ratio of 1.18–1.70 at 40% steam concentration. While the overall ratio of CO/CO_2 was always higher than that from the value from the feed (1.12), the ratio decreased with steam addition, indicating the suppressed dry reforming pathway.

Table 2. The effect of steam concentration during the SCR of bio-syngas.

Steam, %	CH_4 Conv.,%	Changes in Mole Fraction				H_2/CO [1] (overall [2])	Overall CO/CO_2 [3]
		ΔCH_4	ΔCO	ΔCO_2	$\Delta H_2(\Delta CH_4 x2)$		
0	51.9	−6.2	17.0	−11.9	6.6 (12.3)	0.39 (0.87)	3.10
20	55.5	−6.6	10.7	−4.8	13.8 (13.2)	1.29 (1.19)	1.79
40	81.1	−9.7	7.4	2.5	28.0 (19.4)	3.78 (1.70)	1.24

Reaction condition: 850 °C; GHSV = 7.6 × 10^4 h^{-1}, [1]: the ratio of H_2/CO based on the net change from the dry feed. [2]: the overall H_2/CO ratio from dry feed = 1.18; [3]: the overall CO/CO_2 ratio from dry feed = 1.12.

In Figure 7, the changes in the ratio of products upon steam addition were plotted together with the thermodynamic equilibrium values at the temperature of 850 °C. In overall, the addition of steam led to the increase in the production of H_2 and CO_2, which in turn increased the H_2/CO ratio and decreased the CO/CO_2 ratio. Due to the non-equilibrium characteristics in this condition, there was a relatively large discrepancy between the experimental and the thermodynamic values for the overall ratio of CO/CO_2 and net ratio of H_2/CO at the absence of steam and 40% steam addition, respectively. For the ratio of CO/CO_2, it becomes less significant with increasing steam concentration whereas the net ratio of H_2/CO increased the discrepancy with steam addition. In the absence of steam, the dry reforming (R1) was more controlled by mass transfer to reduce the ratio of CO/CO_2. With 40% steam addition, the steam involved reactions (i.e., R2 and R3) were more influenced by mass transfer to limit hydrogen production, which in turn decreased the CO/CO_2 ratio. In other words, depending on the steam addition, some reactions tended to be more significantly influenced by diffusion limitation, which will affect the ratios between products.

3.6. Stability of Rh/Alumina Foam Monolith

Figure 8 shows the XRD patterns for the fresh and spent Rh alumina samples together with gamma-alumina for comparison. According to the visual observation, freshly calcined Rh_2O_3/Al_2O_3 sample has no appreciable change compared to a blank α-Al_2O_3. This may indicate that Rh particles have been well dispersed on the surface of alumina. After being used in the SCR of bio-syngas at 850 °C, the detection of the peaks assigned for Rh (111), (200) and (220) planes [50,51] indicated the presence of metallic Rh on the surface of alumina. However, the exposure to high temperature led to the sintering of Rh particles on the surface after the reaction.

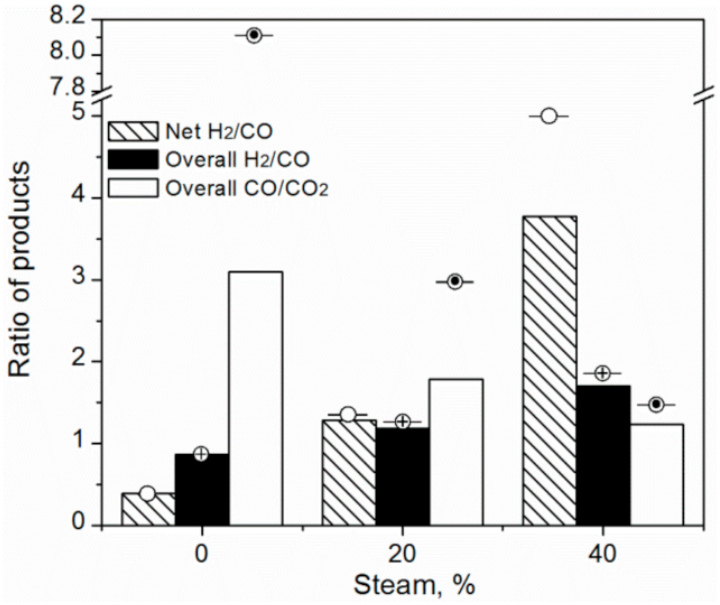

Figure 7. Comparison in the ratios of H_2/CO and CO/CO_2 as a function of the steam concentration between the values from experiments (columns) and those from the thermodynamic equilibrium (symbols with bar) at 850 °C.

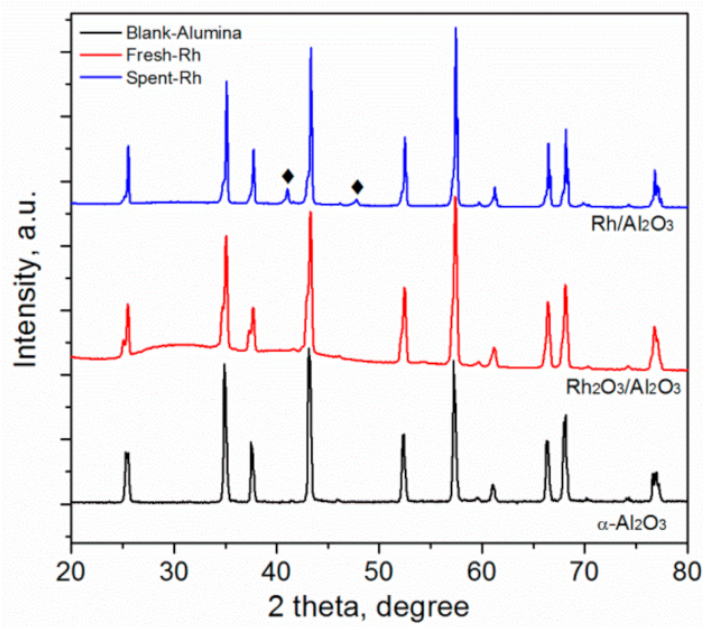

Figure 8. XRD patterns of a blank α-Al_2O_3, fresh and spent Rh/Al_2O_3 samples (♦: metallic Rh).

4. Conclusions

This study investigated the influence of steam addition on the reforming of bio-syngas using Rh-loaded alumina foam monolith catalysts, with which was compared with thermodynamic equilibrium simulation. At 40% steam addition, steam reforming and WGS reaction were prevailed at the temperature below 640 °C, above which dry reforming and r-WGS reaction were gradually intensified. Correspondingly, the ratios of H_2/CO and CO/CO_2 approached the thermodynamic values with temperature. Transition temperature was observed at 640 °C, where E_a was substantially changed. At this transition, the methane conversion reaction during the reforming of bio-syngas seems to shift from the kinetic controlled region to the diffusion controlled region. At 20% steam addition, the increase in the gas velocity intensified the contribution of steam reforming, which in turn increased the

ratio of H_2/CO. Without steam, dry reforming is the main pathway for methane conversion and CO production was maximised due to prevailed R-WGS. According to the comparison of the product ratios from the upgrading process with those from thermodynamic values, main reaction pathways dependent on steam concentration seem to be more affected by diffusion control. This study demonstrated that alumina foam monolith supported metal catalyst could be used in the upgrading of raw bio-syngas with a good stability. It is also recommended that other aspects of foam monoliths catalyst such as different morphology or porosity are investigated towards the upgrading of bio-syngas.

Author Contributions: W.J.L., C.L. and J.P. participated in designing of the study and conducting experiments. W.J.L. contributed to conduct experiments, interpret the outcomes and summarized it. W.J.L. led the preparation of the manuscript. C.L. was partially involved in operating experiments and C.L. conducted the simulation of bio-syngas reforming using ASPEN analysis. J.P. initiated this study and supervised the overall process. C.L. and J.P. also contributed in preparing the manuscript. All authors have read and agreed to the published version of the manuscript.

Funding: This research was conducted with the aid of CSIRO internal support. No external funding was provided.

Institutional Review Board Statement: Not applicable.

Informed Consent Statement: Not applicable.

Data Availability Statement: Data available in a publicly accessible repository.

Acknowledgments: The support of this work by CSIRO is gratefully acknowledged. The authors thank Jarrod Newnham (CSIRO Energy) for assistance with the X-ray diffraction analysis.

Conflicts of Interest: The authors declare no conflict of interest.

References

1. Carlu, E.; Truong, T.; Kundevski, M. *Biogas Opportunities for Australia*; ENEA Consulting: Melbourne, Australia, 2019.
2. Korberg, A.D.; Skov, I.R.; Mathiesen, B.V. The role of biogas and biogas-derived fuels in a 100% renewable energy system in Denmark. *Energy* **2020**, *199*, 117426. [CrossRef]
3. International Energy Agency. *Global Energy & CO2 Status Report 2018*; International Energy Agency: Paris, France, 2018.
4. Intergovernmental Panel on Climate Change. *Special Report on Global Warming of 1.5C*; Intergovernmental Panel on Climate Change: Geneva, Switzerland, 2018.
5. Huber, G.W.; Iborra, S.; Corma, A. Synthesis of transportation fuels from biomass: Chemistry, catalysts, and engineering. *Chem. Rev.* **2006**, *106*, 4044–4098. [CrossRef] [PubMed]
6. Zinoviev, S.; Muller-Langer, F.; Das, P.; Bertero, N.; Fornasiero, P.; Kaltschmitt, M.; Centi, G.; Miertus, S. Next-Generation Biofuels: Survey of Emerging Technologies and Sustainability Issues. *ChemSusChem* **2010**, *3*, 1106–1133. [CrossRef]
7. Alonso, D.M.; Bond, J.Q.; Dumesic, J.A. Catalytic conversion of biomass to biofuels. *Green Chem.* **2010**, *12*, 1493–1513. [CrossRef]
8. Li, C.Z. Special issue-Gasification: A route to clean energy. *Process Saf. Environ. Prot.* **2006**, *84*, 407–408. [CrossRef]
9. Zhang, R. Catalytic destruction of tar in biomass derived producer gas. *Energy Convers. Manag.* **2004**, *45*, 995–1014. [CrossRef]
10. Coll, R.; Salvado, J.; Farriol, X.; Montane, D. Steam reforming model compounds of biomass gasification tars: Conversion at different operating conditions and tendency towards coke formation. *Fuel Process. Technol.* **2001**, *74*, 19–31. [CrossRef]
11. Corella, J.; Toledo, J.M.; Padilla, R. Catalytic hot gas cleaning with monoliths in biomass gasification in fluidized beds. 3. Their effectiveness for ammonia elimination. *Ind. Eng. Chem. Res.* **2005**, *44*, 2036–2045. [CrossRef]
12. Corella, J.; Toledo, M.; Padilla, R. Catalytic hot gas cleaning with monoliths in biomass gasification in fluidized beds. 1. Their effectiveness for tar elimination. *Ind. Eng. Chem. Res.* **2004**, *43*, 2433–2445. [CrossRef]
13. Anis, S.; Zainal, Z.A. Tar reduction in biomass producer gas via mechanical, catalytic and thermal methods: A review. *Renew. Sustain. Energy Rev.* **2011**, *15*, 2355–2377. [CrossRef]
14. Abdoulmoumine, N.; Adhikari, S.; Kulkarni, A.; Chattanathan, S. A review on biomass gasification syngas cleanup. *Appl. Energy* **2015**, *155*, 294–307. [CrossRef]
15. Chattanathan, S.A.; Adhikari, S.; Taylor, S. Conversion of carbon dioxide and methane in biomass synthesis gas for liquid fuels production. *Int. J. Hydrogen Energy* **2012**, *37*, 18031–18039. [CrossRef]
16. Wang, C.G.; Wang, T.J.; Ma, L.L.; Gao, Y.; Wu, C.Z. Steam reforming of biomass raw fuel gas over NiO-MgO solid solution cordierite monolith catalyst. *Energy Convers. Manag.* **2010**, *51*, 446–451. [CrossRef]
17. Choudhary, V.R.; Mondal, K.C. CO_2 reforming of methane combined with steam reforming or partial oxidation of methane to syngas over NdCoO3 perovskite-type mixed metal-oxide catalyst. *Appl. Energy* **2006**, *83*, 1024–1032. [CrossRef]

18. Koo, K.Y.; Roh, H.S.; Jung, U.H.; Yoon, W.L. CeO2 Promoted Ni/Al2O3 Catalyst in Combined Steam and Carbon Dioxide Reforming of Methane for Gas to Liquid (GTL) Process. *Catal. Lett.* **2009**, *130*, 217–221. [CrossRef]
19. Jang, W.J.; Jeong, D.W.; Shim, J.O.; Kim, H.M.; Roh, H.S.; Son, I.H.; Lee, S.J. Combined steam and carbon dioxide reforming of methane and side reactions: Thermodynamic equilibrium analysis and experimental application. *Appl. Energy* **2016**, *173*, 80–91. [CrossRef]
20. Haryanto, A.; Fernando, S.D.; Pordesimo, L.O.; Adhikari, S. Upgrading of syngas derived from biomass gasification: A thermodynamic analysis. *Biomass Bioenergy* **2009**, *33*, 882–889. [CrossRef]
21. Artz, J.; Muller, T.E.; Thenert, K.; Kleinekorte, J.; Meys, R.; Sternberg, A.; Bardow, A.; Leitner, W. Sustainable Conversion of Carbon Dioxide: An Integrated Review of Catalysis and Life Cycle Assessment. *Chem. Rev.* **2018**, *118*, 434–504. [CrossRef]
22. Giuntoli, J.; Agostini, A.; Edwards, R.; Marelli, L. *Solid and Gaseous Bioenergy Pathways: Input Values and GHG Emissions. Calculated According to COM(2016) 767, Ver 2*; EUR 27215 EN; European Commission, Joint Research Centre: Ispra, Italy, 2017.
23. Cybulski, A.; Moulijn, J.A. Monoliths in heterogeneous catalysis. *Catal. Rev.-Sci. Eng.* **1994**, *36*, 179–270. [CrossRef]
24. Twigg, M.V.; Richardson, J.T. Fundamentals and applications of structured ceramic foam catalysts. *Ind. Eng. Chem. Res.* **2007**, *46*, 4166–4177. [CrossRef]
25. Renken, A.; Kiwi-Minsker, L. Microstructured Catalytic Reactors. *Adv. Catal.* **2010**, *53*, 47–122.
26. Mills, P.L.; Quiram, D.J.; Ryley, J.F. Microreactor technology and process miniaturization for catalytic reactions-A perspective on recent developments and emerging technologies. *Chem. Eng. Sci.* **2007**, *62*, 6992–7010. [CrossRef]
27. Richardson, J.T.; Garrait, M.; Hung, J.K. Carbon dioxide reforming with Rh and Pt-Re catalysts dispersed on ceramic foam supports. *Appl. Catal. A-Gen.* **2003**, *255*, 69–82. [CrossRef]
28. Nacken, M.; Ma, L.; Heidenreich, S.; Verpoort, F.; Baron, G.V. Development of a catalytic ceramic foam for efficient tar reforming of a catalytic filter for hot gas cleaning of biomass-derived syngas. *Appl. Catal. B-Environ.* **2012**, *125*, 111–119. [CrossRef]
29. Wang, C.G.; Wang, T.J.; Ma, L.L.; Gao, Y.; Wu, C.Z. Partial oxidation reforming of biomass fuel gas over nickel-based monolithic catalyst with naphthalene as model compound. *Korean J. Chem. Eng.* **2008**, *25*, 738–743. [CrossRef]
30. Rostrupnielsen, J.R.; Hansen, J.H.B. CO_2-Reforming of methane over transition-metals. *J. Catal.* **1993**, *144*, 38–49. [CrossRef]
31. Wang, Y.; Chin, Y.H.; Rozmiarek, R.T.; Johnson, B.R.; Gao, Y.; Watson, J.; Tonkovich, A.Y.L.; Vander Wiel, D.P. Highly active and stable Rh/MgO-Al2O3 catalysts for methane steam reforming. *Catal. Today* **2004**, *98*, 575–581. [CrossRef]
32. Meille, V. Review on methods to deposit catalysts on structured surfaces. *Appl. Catal. A-Gen.* **2006**, *315*, 1–17. [CrossRef]
33. Richardson, J.T.; Paripatyadar, S.A. Carbon dioxide reforming of methane with supported rhodium. *Appl. Catal.* **1990**, *61*, 293–309. [CrossRef]
34. Zhang, K.; Jiang, X. An investigation of fuel variability effect on bio-syngas combustion using uncertainty quantification. *Fuel* **2018**, *220*, 283–295. [CrossRef]
35. Zhang, K.; Lupo, G.; Duwig, C. Investigation of wet combustion instability due to bio-syngas fuel variability. *Fuel* **2021**, *285*, 119120. [CrossRef]
36. Lu, Y.J.; Lee, T. Influence of the feed gas composition on the Fischer-Tropsch synthesis in commercial operations. *J. Nat. Gas Chem.* **2007**, *16*, 329–341. [CrossRef]
37. Yin, X.L.; Leung, D.Y.C.; Chang, J.; Wang, J.F.; Fu, Y.; Wu, C.Z. Characteristics of the synthesis of methanol using biomass-derived syngas. *Energy Fuels* **2005**, *19*, 305–310. [CrossRef]
38. Cullis, C.F.; Willatt, B.M. Oxidation of methane over supported precious metal catalysts. *J. Catal.* **1983**, *83*, 267–285. [CrossRef]
39. Bruno, T.; Beretta, A.; Groppi, G.; Roderi, M.; Forzatti, P. A study of methane partial oxidation in annular reactor: Activity of Rh/alpha-Al2O3 and Rh/ZrO2 catalysts. *Catal. Today* **2005**, *99*, 89–98. [CrossRef]
40. Kolaczkowski, S.T.; Thomas, W.J.; Titiloye, J.; Worth, D.J. Catalytic combustion of methane in a monolith reactor: Heat and mass transfer under laminar flow and pseudo-steady-state reaction conditions. *Combust. Sci. Technol.* **1996**, *118*, 79–100. [CrossRef]
41. Hayes, R.E.; Kolaczkowski, S.T.; Thomas, W.J.; Titiloye, J. Transient experiments and modeling of the catalytic combustion of methane in a monolith reactor. *Ind. Eng. Chem. Res.* **1996**, *35*, 406–414. [CrossRef]
42. Wei, J.M.; Iglesia, E. Structural requirements and reaction pathways in methane activation and chemical conversion catalyzed by rhodium. *J. Catal.* **2004**, *225*, 116–127. [CrossRef]
43. Tonkovich, A.L.Y.; Yang, B.; Perry, S.T.; Fitzgerald, S.P.; Wang, Y. From seconds to milliseconds to microseconds through tailored microchannel reactor design of a steam methane reformer. *Catal. Today* **2007**, *120*, 21–29. [CrossRef]
44. Kuznetsov, V.V.; Vitovsky, O.V.; Gasenko, O.A. Methane steam reforming in an annular microchannel with Rh/Al2O3 catalyst. *J. Eng. Thermophys.* **2009**, *18*, 187–196. [CrossRef]
45. Panagiotopoulou, P.; Kondarides, D.I.; Verykios, X.E. Selective methanation of CO over supported noble metal catalysts: Effects of the nature of the metallic phase on catalytic performance. *Appl. Catal. A-Gen.* **2008**, *344*, 45–54. [CrossRef]
46. Qin, D.Y.; Lapszewicz, J.; Jiang, X.Z. Comparison of partial oxidation and steam-CO_2 mixed reforming of CH4 to syngas on MgO-supported metals. *J. Catal.* **1996**, *159*, 140–149. [CrossRef]
47. Oyama, S.T.; Hacarlioglu, P.; Gu, Y.; Lee, D. Dry reforming of methane has no future for hydrogen production: Comparison with steam reforming at high pressure in standard and membrane reactors. *Int. J. Hydrogen Energy* **2012**, *37*, 10444–10450. [CrossRef]
48. Ozkara-Aydinoglu, S. Thermodynamic equilibrium analysis of combined carbon dioxide reforming with steam reforming of methane to synthesis gas. *Int. J. Hydrogen Energy* **2010**, *35*, 12821–12828. [CrossRef]

49. Avraam, D.G.; Halkides, T.I.; Liguras, D.K.; Bereketidou, O.A.; Goula, M.A. An experimental and theoretical approach for the biogas steam reforming reaction. *Int. J. Hydrogen Energy* **2010**, *35*, 9818–9827. [CrossRef]
50. Fiedorow, R.M.J.; Wanke, S.E. Effect of gamma-alumina crystallinity on the state of rhodium during high-temperature treatments in oxygen and hydrogen. *Appl. Catal. B-Environ.* **1997**, *14*, 249–259. [CrossRef]
51. Ziegelbauer, J.M.; Gulla, A.F.; O'Laoire, C.; Urgeghe, C.; Allen, R.J.; Mukerjee, S. Chalcogenide electrocatalysts for oxygen-depolarized aqueous hydrochloric acid electrolysis. *Electrochim. Acta* **2007**, *52*, 6282–6294. [CrossRef]